Carbon 99 (2016) 423–431

Contents lists available at ScienceDirect

Carbon

journal homepage: www.elsevier.com/locate/carbon

The mechanism of direct laser writing of graphene features into graphene oxide films involves photoreduction and thermally assisted structural rearrangement

Rakesh Arul [a, b, c], Reece N. Oosterbeek [a, b, c], John Robertson [e], Guangyuan Xu [b], Jianyong Jin [b], M. Cather Simpson [a, b, c, d, *]

[a] The Photon Factory, The University of Auckland, Private Bag 92019, New Zealand
[b] School of Chemical Sciences, The University of Auckland, Private Bag 92019, New Zealand
[c] The MacDiarmid Institute for Advanced Materials and Nanotechnology, The Dodd Walls Centre for Quantum and Photonic Technologies, New Zealand
[d] Department of Physics, The University of Auckland, Private Bag 92019, New Zealand
[e] School of Applied Sciences, Auckland University of Technology, Auckland, New Zealand

ARTICLE INFO

Article history:
Received 5 September 2015
Received in revised form
14 December 2015
Accepted 14 December 2015
Available online 17 December 2015

ABSTRACT

Photoreduction of graphene oxide (GO) to reduced graphene oxide (rGO) under ambient conditions was evaluated for three laser processing approaches: 800 nm fs pulses, 248 nm ns pulses, and 788 nm continuous wave (CW) illumination. Resultant features were compared using Raman, XPS, optical profilometry and SEM. The most effective approach for photoreduction and graphenization with minimal defects was nanosecond processing (0.12 J cm^{-2}; 40 pulses overlapped). The Raman 2D band intensity confirmed a graphene-like structure. The ablation threshold for GO (248 nm, 5 ns) is ~10 mJ cm^{-2}. Laser photoreduction with CW 788 nm yielded similar oxygen removal, but conversion to a graphene-like structure was poorer, and more defects were introduced. Femtosecond pulse illumination resulted in oxygen removal from the surface but the transformation to an sp^2 graphene-like structure was not observed. This result suggests that the photochemical reduction of GO is not thermally mediated, but the structural reorganization from sp^3 to sp^2 requires heat deposition into the material. This is the first such comparison on a consistent GO substrate under comparable ambient conditions, and the results provide insight into the fundamental mechanism and the utility of the method for direct laser writing electronically active materials.

1. Introduction

The promise of graphene as a next-generation material has been fulfilled in myriad ways since its discovery in 2004 [1] and the Nobel Prize awarded for this in 2010 [2]. In addition to its current uses, growing by the day, graphene has also provided impetus for research into the wider field of two-dimensional materials in a "post-graphene age" [3].

Many of the applications of graphene arise from its unique properties [4,5]. It has an extremely high carrier mobility, thermal conductivity and Young's modulus. Electronic transport in graphene is exceptionally fast; the electrons behave as massless Dirac fermions and travel at close to the effective speed of light in the lattice [6], providing condensed matter physicists an interesting framework within which to test known theories and discover new ones.

The industrial motivations to use graphene are strong, and hence production methods must keep pace with graphene's emerging applications and be tailored for its behaviour. Graphene has been produced via the famous Scotch-tape method (mechanical exfoliation of graphite) [1], epitaxial growth [7], shear-exfoliation of graphite flakes in liquids [8], chemical vapour deposition [9] and a suite of methods that attempt to transform graphene oxide to graphene by reduction [5,10].

In the latter approaches, graphite is first oxidised to generate graphite oxide, which is then dispersed via sonication into graphene oxide (GO) monolayers in water to form a stable aqueous colloid [11,12]. GO can be cast into films [13] and deposited on various surfaces [14,15]. Additionally, the dispersed GO can be

* Corresponding author.
E-mail address: c.simpson@auckland.ac.nz (M.C. Simpson).

http://dx.doi.org/10.1016/j.carbon.2015.12.038
0008-6223/

functionalized via its oxygen-containing surface groups [16,17] with, for example, isocyanates [18], nanoparticles [19], enzymes [20] and other biomolecules [21]. This is advantageous in the production of biosensors [22,23] and tissue engineering substrates [23], for example. In contrast to GO, graphene and graphite are both insoluble in water, difficult to cast onto films via conventional liquid-phase chemistry and chemically challenging to functionalize. GO thus has significant advantages as a starting material for direct laser writing of electronically active structures into surfaces.

The oxygen atoms in GO disrupt the material from graphene's planar, hexagonal conformation. The consequence of this structural difference is that GO is an insulator. The approach, then, to obtaining graphene's structure and its extraordinary functionality, is to remove the oxygen atoms in GO by reduction, and allow the carbon atoms to relax back into the graphene conformation.

The main methods for reducing GO are chemical, thermal, and photoreduction. Reduced graphene oxide (rGO) has found uses in the areas spanning the breadth of materials science and engineering, with examples like field-effect transistors [24], photovoltaic devices [25], supercapacitors [26], 3D holographic images [27] and chemical sensors [28], just to name a few. It should be noted though, that although the reduction of GO provides an effective route to monolayers of graphene, the final processed material generally consists of patches of pristine graphene connected by unreduced, oxygen-containing, carbon groups [29]. Additionally, the reduction process can introduce defects (e.g. heptagons, pentagons, edges [30]) into the final rGO structure [31], the degree to which depends on the method of reduction. Hence, we and others formally distinguish rGO from graphene.

Defects in the graphene structure, as in rGO, are not necessarily disadvantageous, despite the concomitant reduction in electrical conductivity. Point and line-type defects present in polycrystalline graphene [30] and nanometre-scale topological defects in rGO [32] can be beneficial for Li ion batteries, for example. Pyridinic-type extended defects in N-doped graphene increase the capacity of the material for Li adsorption beyond that of pristine N-doped graphene [33]. Similarly, divacancy defects can act as seed points for the intercalation of Li ions [34]. Defects also appear to increase the adsorption of various gas molecules [35–37], and thereby enhance the use of graphene-like materials in gas sensing. Indeed, the chemical functionalization routinely performed on GO and rGO, considered defects by many [38], can confer significant benefits for applications [39]. Such applications exploit the trade-off between the increased electrocatalytic activity and loss of conductivity from a defect site [40].

For some applications, pristine graphene is more suitable. The presence of any kind of defect in a highly conductive network of sp^2 carbons introduces a scattering centre for electrons and hence the electrical conductivity suffers on the nanoscale [41]. Some applications that require complete graphenisation include electromechanical actuators [42], surface-enhanced Raman spectroscopy [43], and Pd nanoparticle-assisted electro-catalysis [44].

Photoreduction has distinct advantages compared to the chemical and thermal reduction methods [45]. It is solvent and harsh chemical free; the reduction performed entirely in the solid state and is aligned with the principles of green chemistry. Additionally, in a single step, it allows reduction of the GO layer and simultaneous patterning without the need for masks or complex processing [46]. Using lasers and micromachining stages, one can directly laser-write micron-scale patterns into GO films. This potential immediately lends itself to applications such as electrodes for supercapacitors, sensors, flexible electronics and circuits. rGO has a resistivity of 80–500 Ω/sq [45], orders of magnitude smaller than that of GO (typically > 20 MΩ/sq) [47]. Hence conductive circuits can be easily and reliably patterned onto the surface of flexible GO substrates, thereby linking the production method (direct-write laser reduction) to the rGO application (microelectronics).

This work focuses on the photoreduction of GO to rGO with lasers. The goals are to understand the mechanism in this promising approach, and to determine optimal conditions for direct laser-writing of rGO microstructures. We qualitatively and quantitatively compare the effectiveness of the three most common laser direct-write methods: (1) nanosecond UV (248 nm) pulses, (2) 788 nm CW illumination, and (3) 100 fs, near infrared (800 nm) pulses. We use x-ray photoelectron spectroscopy (XPS), Raman spectroscopy, optical profilometry and scanning electron microscopy (SEM) to thoroughly characterize the laser treated surfaces. Raman spectroscopy is an important tool for quantifying the extent of the sp^3 to sp^2 transformation that accompanies photoreduction, through the intensity of the 2D Raman band [46,48,49]. Finally, our experiments are under ambient conditions, as this offers the most scalable approach to rGO production.

Previous research by others has demonstrated the viability and utility of rGO produced via direct laser writing [36,46,47,49–54]. However, these experiments were either performed in a high purity inert gas or high vacuum environment [46,49,50,52,53], with different lasers on different substrates [47,54] or without consideration of the Raman 2D band to confirm that the photoreduced material has adopted the important sp^2 structural form of graphene [36,51]. This paper is thus the first of its kind to compare the common laser photoreduction methods under common conditions, upon a common GO substrate, and to confirm the extent of both photoreduction and conformational transformation of the rGO formed.

2. Materials and methods

2.1. Production of graphene oxide (GO) films

Two different forms of GO were utilised to make films for laser photoreduction. The first was synthesized via the modified Hummers method [55,56]. The second was purchased from a commercial source (Graphenea Inc., USA). Films of each were made by drop-casting 12 mL of 3.7 mg mL^{-1} aqueous GO onto biaxially oriented polyethylene terephthalate (PET) films (Mylar, RS Components). The films were dried under ambient conditions for 24 h, in a Class 100 cleanroom. PET was chosen because of its flexibility and suitability as a substrate for supercapacitors. The resulting GO films have not degraded in air, at 20–25 °C for over 5 months. Investigation of the surface morphology by optical profilometry also revealed an inherent average surface roughness of 1.0–1.7 μm.

2.2. Laser photoreduction techniques

Three laser sources were used to direct-write rGO into the GO films. All of these laser treatments were performed at room temperature (20 °C) at ambient pressure and 30% relative humidity.

The CW, 788 nm laser (LightScribe DVD drive, Hewlett–Packard Inc., USA) was used under maximum contrast settings in order to increase the extent of reduction, guided by the work of Strong et al. [47]. The GO film on PET was adhered to the surface of a LightScribe-enabled DVD using spray adhesive (3M Spraymount repositionable adhesive). Multiple 1.5 cm × 1.5 cm processed areas were scribed; each sample was exposed to six passes in the LightScribe DVD device. The process was controlled using the LightScribe Direct Disk Labelling software.

Nanosecond, UV laser reduction was performed with a Xantos XS laser (248 nm, 5 ns pulse duration, 500 Hz repetition rate, Coherent Inc., USA) with a range of incident fluence and pulse

overlap conditions. The laser was directed to a commercial micromachining stage (IX-100C, JPSA Inc., USA) for controlled illumination of the GO film. A mask was employed to generate an approximately flat-top intensity profile in a 50 μm × 50 μm square spot at the GO sample surface. Fluence values from 48 mJ cm^{-2} to 240 mJ cm^{-2} were employed. The number of pulses overlapped at each point in the sample ranged from 2 to 50.

Femtosecond laser reduction (800 nm, 100 fs pulse duration, 1 kHz Legend Elite, Coherent Inc., USA) was carried out with a Ti:Sapphire amplified laser. The pulse train was directed to the micromachining stage (IX-100C, JPSA Inc., USA). At the sample surface, the masked beam was demagnified to a 50 μm × 50 μm square spot with an approximately flat-top intensity profile. The fluence ranged from 47 mJ cm^{-2} to 968 mJ cm^{-2} (1.17–24.2 μJ $pulse^{-1}$). As with the nanosecond laser processing, the number of pulses overlapped at each point in the sample ranged from 2 to 50.

2.3. Characterisation techniques

Raman spectroscopy was performed with an alpha300 R confocal Raman microscope (WiTEC GmbH, Germany; 532 nm, incident power = 0.288 mW). For each photoreduction condition, Raman spectroscopic analysis was performed on at least 5 different areas on an array of machined 50 μm × 50 μm spots.

Samples for XPS analysis were prepared by scribing lines on the GO surface and adjusting the scribing rate to change the pulse overlap. XPS was carried out on an Axis ultraDLD (Kratos Ltd., UK), using a monochromated Al Kα X-ray source with a power of 100 W. The chamber pressure was on the order of 10^{-9} torr and core level scans were carried out at a pass energy of 20 eV. The data was fit using the CasaXPS software (Casa Software Ltd., USA); spectral components were fit using Gaussian–Lorentzian functions and asymmetric Gaussian–Lorentzian components for the carbon sp^2 peaks [57].

An SEM (JEOL JCM6000, Coherent), stylus-contact profiler (DektakXT, Bruker Inc., USA) and optical profiler (Bruker Contour GTK, Bruker Inc., USA) were used to characterise the surface morphology and thickness of the GO and rGO films. They were all approximately 20–25 μm thick. The optical profiler was used in the vertical scanning interferometry mode. The optical profiler and the SEM also were used to analyse the diameters and depths of machined holes in the GO film, in order to determine the UV nanosecond pulse laser ablation threshold.

Glancing angle x-ray diffraction (GAXRD) data was collected using a PANalytical X'Pert Pro diffractometer located at Victoria University of Wellington (New Zealand). This instrument uses a Cu Kα X-ray source. Glancing angle experiments were carried out with incident angle ω = 1°, with a 2θ scan range from 5 to 35°, step size of 0.02°, and acquisition time of 15 s per step.

2.4. Ablation threshold determination

The fluence threshold for UV nanosecond pulse laser ablation was determined using the volume regression technique [58–60]. Lines were machined at various fluence levels and overlapping pulse conditions, and their depths measured using optical profilometry.

3. Results and discussion

In this work, we quantify the extent and quality of the laser photoreduction and conversion to a graphene-like structure when GO is irradiated to form rGO. We compare the performance of the three most widely used laser systems for direct-writing of rGO features. Raman spectroscopy and XPS provided information about the surface chemical and physical characteristics; optical profilometry and SEM provided insight into the morphology of the irradiated surfaces.

Raman spectroscopy is an excellent tool for analysing graphene, GO and rGO [48,61,62]. Three main Raman spectral features are useful for our study. The G-band (~1580 cm^{-1}) appears in graphene, GO and rGO and reflects scattering from an in-plane, E_{2g} phonon. In this study, we use it to normalize our Raman spectra, and thereby enable comparisons of the relative intensities of the other bands in the spectra.

The Raman D-band (~1350 cm^{-1}) is an A_{1g} phonon associated with an sp^2 ring-breathing mode. This band would be an excellent marker for graphene-like structure, however it is largely silent because of the Raman selection rules of the system. It gains intensity in the spectrum when there are defects in the surface layers of the film [63].

In contrast, the first overtone of this band, the 2D band (2700 cm^{-1}) is an allowed transition, and appears in the spectrum when the sp^2 rings are present. This 2D band is inextricably linked to the electronic band structure of graphene, and changes as graphene's band structure does [48]. The oxygen groups in GO give rise to a large reduction in the number of sp^2 hybridized carbons, and hence we observe no appreciable 2D band intensity in the Raman spectra of our GO films. Upon photoreduction and relaxation of the conformation of the carbon lattice to the more graphene-like, sp^2 structure, the 2D Raman intensity increases. Our choice to rely on the intensity of the 2D band as the best indicator of few-layer graphene is supported by the work of Sokolov et al. [46]. and Trusovas et al. [49].

The ratios of the intensities of the D and G peaks (I_D/I_G) and of the 2D and G peaks (I_{2D}/I_G) in the Raman spectra of our surfaces thus reflect the defect density and extent of graphenization – photoreduction and conversion to a graphene-like structure – respectively, of the surface before and after laser illumination. Ideally, we want to optimize for minimum defect introduction and maximum photoreduction and graphenization (low I_D/I_G and high I_{2D}/I_G).

XPS reflects the elemental ratios of the chemical binding states within the first few layers in the film. XPS is an extremely surface-sensitive technique and is well suited for evaluating the formation of rGO in our laser treated GO thin-films. In the survey spectrum, a greater extent of reduction is shown by an increase in the carbon to oxygen (C:O) ratio. In the chemical state scans, the C1s XPS spectral bands for the epoxide/hydroxyl (286 eV), carbonyl (288 eV), and carboxyl groups (289 eV) will depend upon the oxygen content of the surface, and thus the extent of photoreduction [62], when compared to the C–C (sp^2 and sp^3) band at ~285 eV. XPS is less sensitive to the structural conversion to the planar sp^2 network of the surface.

In the results and discussion below, the processed area of the sample is identified by the type of laser employed: femtosecond pulses (fs-rGO), nanosecond pulses (ns-rGO) and continuous wave illumination (cw-rGO).

3.1. Comparison of the GO to graphene-like rGO transformation induced by CW, ns and fs laser pulses

Laser photoreduction and graphenization of GO to rGO depends upon the laser parameters employed during processing. For the continuous wave (788 nm) approach, we used the most effective settings of the LightScribe system, as determined by Ref. [47].

The ns-rGO generation was sensitive to the laser parameters (number of pulses overlapped, incident laser fluence) under the range of conditions that we employed. Fig. 1 shows the I_{2D}/I_G ratio

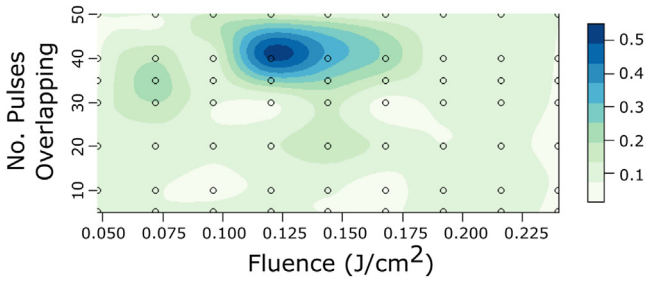

Fig. 1. The Raman I_{2D}/I_G ratio measured on ns-rGO samples versus incident laser fluence and number of overlapping pulses. White dots represent data; contours were fit by local polynomial regression.

as a function of both the number of pulses overlapped and the incident laser fluence. The best photoreduction and formation of sp^2 conformations was observed at 0.12 J cm^{-2} and for 40 pulses overlapped at each spot (Fig. 1).

In contrast, exploration of the parameter space for femtosecond (800 nm) laser processing of GO showed no apparent dependence of the GO to rGO transformation upon these parameters (see Supplementary Material). Below, then, we compare results of experiments performed under optimal continuous wave (788 nm) and nanosecond pulse (248 nm) conditions, and set the femtosecond pulse (800 nm) laser parameters to be 0.15 J cm^{-2} and 40 overlapping pulses, similar to those used for the nanosecond laser processing.

3.1.1. XPS chemical state scans

Significant differences among unprocessed GO and the fs-rGO, ns-rGO and cw-rGO samples were observed in the XPS chemical state scans (Fig. 2). A clear decrease in the intensities of the oxygen containing peaks relative to the major carbon dominated band at 284.5 eV was observed for all three laser processed samples. This result indicates that oxygen is being removed from the surface of GO during laser exposure during UV ns, nIR fs and nIR CW laser processing.

Comparisons among the XPS spectra of fs-rGO, ns-rGO and cw-rGO shows that the nanosecond (248 nm) and continuous wave (788 nm) laser processes were approximately equally effective in photoreduction, and both are more efficient than are the femtosecond (800 nm) pulses under the conditions employed. Table 1 provides detailed comparisons among the constituent bands in the XPS spectra, normalized to the intensity of the carbon signal (sp^2 and sp^3) at 284.5 eV, to highlight the loss of oxygen atoms from the surface.

The XPS evidence suggests that the photoremoval of oxygen from the surface depends upon the laser method used. When femtosecond pulses are used, the intensities of the carbonyl (287 eV) and carboxyl (289 eV) bands decrease proportionally more than does the epoxide/hydroxyl peak (285.5 eV). A detailed comparison shows enrichment of the epoxide/hydroxyl groups (over C═O and C(═O)O) in fs-rGO over untreated GO (ratio of epoxide/hydroxyl groups to [C═O + C(═O)O] increases from 2.34 for GO to 2.63 for fs-rGO); Table 1. The opposite is observed in ns-rGO and cw-rGO; the two higher energy bands sum to approximately the same total intensity as does the lower energy C—O peak (ratio of epoxide/hydroxyl groups to [C═O + C(═O)O] is 1.09 for ns-rGO and 1.15 for cw-rGO). These results indicate that the femtosecond laser pulses preferentially remove oxygen moieties involved in higher energy (e.g. double) bonds.

3.1.2. Raman spectroscopy

As discussed more fully above, the Raman spectra provide insight into the transformation of the carbon surface from the sp^3 conformation characteristic of untreated GO to the sp^2 geometry indicative of graphene like domains (I_{2D}/I_G). In addition, the I_D/I_G ratio is larger when the surface has more defects. Fig. 3 shows the Raman spectra of GO, fs-rGO, ns-rGO and cw-rGO normalized to the G-band intensity; the I_{2D}/I_G and I_D/I_G intensity ratios are summarized in Table 2.

Examination of the I_D/I_G ratios shows that cw-rGO is characterized by significantly higher presence of defects, relative to untreated GO and to both fs-rGO and ns-rGO. Continuous wave illumination thus appears to inflict more damage upon the material, than do either nanosecond or femtosecond pulses.

It is also apparent that the application of nanosecond pulses to GO results in the highest level of graphenization in the rGO product: the I_{2D}/I_G ratio increases by a factor of 6 relative to that seen in untreated GO. The cw-rGO also shows increased sp^2 domains, but to a much lesser extent than is seen in ns-rGO. Finally, the femtosecond laser pulses induce very little, if any, conversion of sp^3 to sp^2 domains in the system. The I_{2D}/I_G for fs-rGO is 0.1, identical to that for untreated GO.

Taken together, the XPS and Raman results strongly suggest that the photoremoval of oxygen and the conversion to the electronically desirable graphene-like structure are linked, but separate, photoinitiated events. This is discussed further below.

3.1.3. Scanning electron microscopy

The microstructures that result from laser treatment of GO depend strongly upon the type of laser employed (Fig. 4). The SEM images show that GO is relatively flat and featureless (Fig. 4a), with sub-10 μm ripples that originate in the GO casting procedure.

In contrast, the surfaces of the laser treated samples exhibit significantly higher surface roughness, with features that vary with the preparation method (Fig. 4b–d). Both femtosecond and nanosecond pulsed laser irradiation created relatively small, irregular (<10 μm diameter) nodules on the surface. For fs-rGO, ripple features are superimposed on these features (Fig. 4b); these are absent on the surface of ns-rGO (Fig. 4c). These ripples may be laser induced periodic surface structures (LIPSS), observed frequently in ultrashort pulse, sub-ablation threshold treatment of materials [64,65]. Exposure of the GO film to continuous wave illumination generated relatively small nodules that are on the order of 10 μm or slightly larger (Fig. 4d).

3.2. UV nanosecond laser photoreduction and graphenization of GO to ns-rGO

Under ambient conditions (20 °C, 30% RH in air), the 248 nm, nanosecond pulses were clearly superior for photoreducing the GO surface, inducing the required structural transformation from sp^3 to sp^2 and resulting in a uniform ns-rGO film with few additional defects.

We identified a relatively narrow set of fluence and pulse overlap conditions that provide optimal conversion of GO to ns-rGO (Fig. 1). Maximum graphenization occurred in the region between about 0.115 and 0.135 J cm^{-2} and 35 to 45 overlapped pulses. A secondary, less effective region is observed at slightly lower fluence and pulse number. The need for multiple pulses to obtain effective creation of the ns-rGO film is consistent with recent findings by Sokolov et al. under conditions of high vacuum [46].

A similar analysis of the I_D/I_G ratio (Fig. 5) shows two regions in this parameter space that lead to higher photoinduced defect formation. Fortunately, both of these regions induce only minor elevations in the I_D/I_G ratio, and neither overlaps completely with the

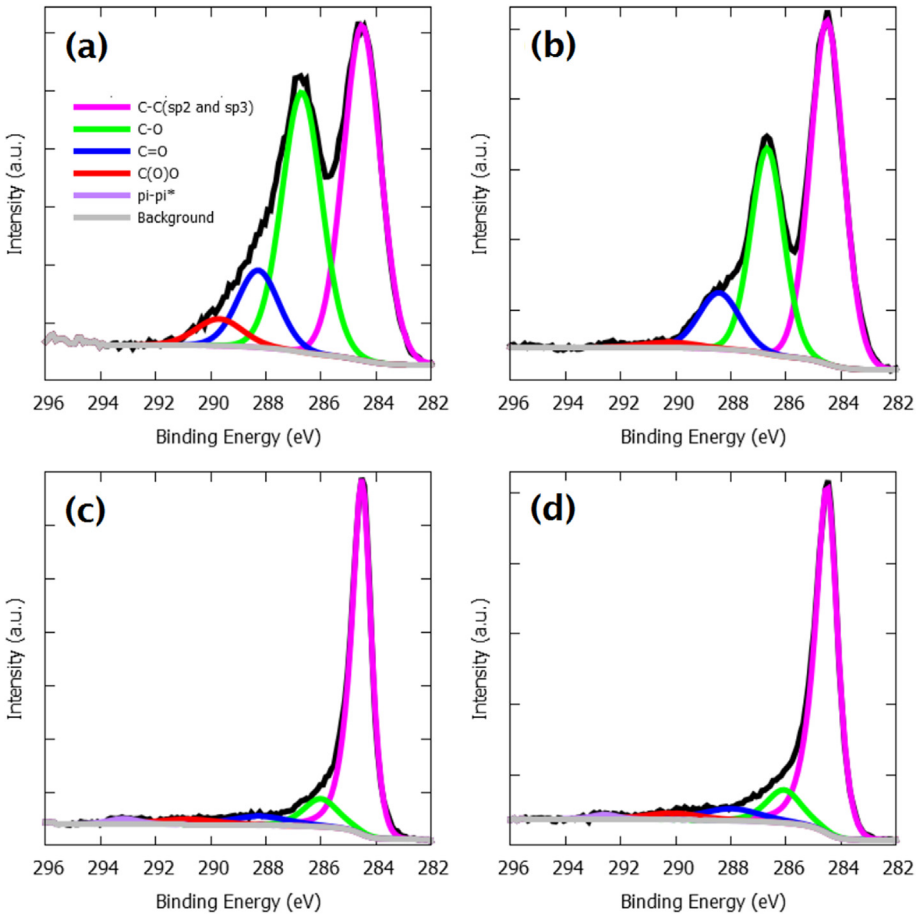

Fig. 2. XPS chemical state scans of (a) GO, (b) fs-rGO (0.15 J cm^{-2}; 40 overlapping pulses), (c) ns-rGO (0.12 J cm^{-2}; 40 overlapping pulses), and (d) cw-rGO (LightScribe maximum contrast, six passes).

Table 1
XPS chemical state components for GO, fs-rGO, ns-rGO and cw-rGO, normalised to the C–C (284.5 eV) peak intensity.

Sample[a]	C–O (285.5 eV)	C=O (287 eV)	C(=O)O (289 eV)	$\pi - \pi^*$ satellite	$\frac{C-O}{[C=O + C(=O)O]}$
GO	0.83	0.25	0.10	–	2.34
fs-rGO	0.59	0.20	0.03	–	2.63
ns-rGO	0.16	0.10	0.05	0.02	1.09
cw-rGO	0.15	0.08	0.05	0.03	1.15

[a] Sample preparation conditions: fs-rGO (0.15 J cm^{-2}; 40 overlapping pulses); ns-rGO (0.12 J cm^{-2}; 40 overlapping pulses); cw-rGO (LightScribe maximum contrast, six passes).

peak conditions for photoreduction and graphenization of GO to ns-rGO. The observation of only minor photoinduced defect formation under ambient conditions with 248 nm ns pulses is consistent with Yung et al. [54]. Some find a laser-induced reduction of defects, as evidenced by I_D/I_G ratios of less than 1.0, but these require vacuum or low pressure inert gas [46,52,53]. The map of the I_D/I_G parameter space obtained is anticipated to be useful in applications where defect introduction and simultaneous reduction is required.

Combining these two results, we have determined an optimum UV nanosecond laser processing condition that induces the largest extent of phototransformation to graphenized ns-rGO while minimizing the introduction of defects: 0.12 J cm^{-2} and 40 overlapped pulses. This optimum condition generates Raman spectra with an I_{2D}/I_G of 0.59 and an I_D/I_G of 1.1 (Table 2).

XPS survey scans of GO and ns-rGO fabricated under the optimal conditions demonstrate that the C:O ratio increases from 2.95 to 10.84 upon laser modification (see Supplementary Material). This 4-fold change represents a marked decrease in the presence of oxygen-containing functional groups at the surface upon processing GO to ns-rGO. The extent is comparable to that obtained by chemical and thermal reduction methods [36,51,52] and by others who have explored UV nanosecond processing of GO under ambient conditions [54].

Our optimum settings for nanosecond laser processing of GO under ambient conditions are promising for future industrial uses, but laser treatment under high vacuum provides superior conversion to ns-rGO. Sokolov et al. observed a 40-fold increase in the C:O ratio under high vacuum (10^{-6} torr) and room temperature, and for similar, though not identical, laser pulses (20 ns, 248 nm, 1 Hz) [46]. Interestingly, the optimal GO to ns-rGO condition obtained in the high vacuum study are similar to the ones we determined under ambient air conditions: 0.132 J cm^{-2} and 32 overlapped pulses [46]. We also see a requirement for pre-pulses. The small variance

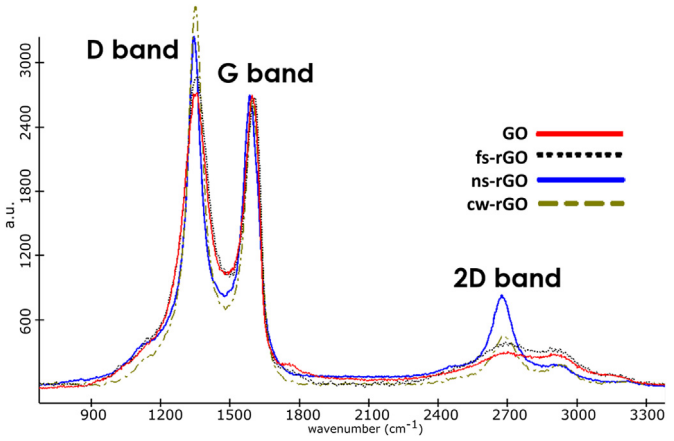

Fig. 3. Average Raman spectra (5 points on the surface) normalized to the G-band intensity. Laser processing conditions: fs-rGO (0.15 J cm^{-2}; 40 overlapping pulses), ns-rGO (0.12 J cm^{-2}; 40 overlapping pulses), and cw-rGO (LightScribe maximum contrast, six passes).

Table 2
Raman I_{2D}/I_G and I_D/I_G ratios GO, fs-rGO, ns-rGO and cw-rGO.

	GO	fs-rGO[a]	ns-rGO	cw-rGO
I_D/I_G	1.0	1.1	1.1	1.3
I_{2D}/I_G	0.10	0.10	0.59	0.17

[a] Sample preparation conditions: fs-rGO (0.15 J cm^{-2}; 40 overlapping pulses); ns-rGO (0.12 J cm^{-2}; 40 overlapping pulses); cw-rGO (LightScribe maximum contrast, six passes).

between the optimal fluences is most likely due to small differences in the GO films or the nanosecond laser pulsewidths. The similarity in optimal processing conditions despite the large differences in the oxygen content of the resultant ns-rGO surfaces suggests the photoreduction and graphenization processes are the same in air and in vacuum. The higher oxygen content in the ns-rGO films processed in air most likely derives from re-deposition of ejected, oxygen-containing material and/or re-functionalization of the photoprocessed surface by oxygen in the atmosphere. This idea is consistent with Sokolov's proposal of plume interactions [46].

3.3. UV nanosecond ablation threshold of GO

The SEM images in Fig. 4c indicate that the optimum laser fluence for photoreduction and graphenization of GO to ns-rGO is above the nanosecond UV laser ablation threshold for this material. In order to assess this properly, we have determined the UV, nanosecond pulsed laser ablation threshold for GO (Fig. 6).

Using the volume regression technique [58–60], the laser ablation threshold for GO using 10 ns, 248 nm laser pulses was found to be about 10 mJ cm^{-2}, about 10-fold lower than the optimal fluence for converting GO to ns-rGO under these conditions. This is the first report of an ablation threshold for GO, to our knowledge. It represents the minimum laser fluence required to change the surface morphology of the GO film.

4. Mechanism of laser reduction of graphene oxide to reduced graphene oxide

The difference in the properties of the rGO films produced by nanosecond and femtosecond pulses provides key insight into the mechanism of the laser induced transformation of GO into a graphene-like, rGO structure. By XPS, we observe the loss of oxygen from the surface during processing by both types of pulses, albeit more efficiently for the nanosecond laser treatment. However, the conversion from sp^3 to sp^2 structures, the graphenization of the surface, is apparent in the Raman spectra (I_{2D}/I_G ratio) for ns-rGO films, but not for their fs-rGO counterparts.

We therefore propose that the mechanism of direct-write laser transformation of GO to graphene (rGO) occurs in two steps: photochemical removal of oxygen from the surface and thermally mediated relaxation of the carbon lattice to a planar, hexagonal sp^2 conjugated, graphene-like layer. This idea is supported by the different mechanisms through which nanosecond and femtosecond pulses interact with materials – femtosecond laser pulses are much less effective at depositing heat in a material than are nanosecond laser pulses [66].

The nanosecond laser pulses photochemically remove oxygen, ablate the material, and in the process also heat the irradiated spot and the area around it (the well-known heat affected zone). The heating provides the local lattice with the energy required to rearrange into graphene-like domains. Essentially, this is a highly localized, laser-mediated, thermal annealing process. The continuous wave laser processing operates in the same way, but because of its wavelength and lower fluence, the deposition of thermal energy in the film is not as high.

The deposition of heat, and hence the thermally mediated structural relaxation, requires a laser pulse with a duration longer than that of the electron-phonon equilibration time of the material. In GO, the electron-phonon equilibration time has been found to be 0.37 ps [67]. The femtosecond pulsed laser we used for reduction has a pulse duration of about 100 fs – the pulse duration is significantly shorter than the time required for the excited electrons to transfer their energy to the phonons and thereby heat the lattice. Hence the same underlying mechanistic reason that femtosecond laser micromachining is a “cold cutting” process [66] leads to the absence of reorganization of the oxygen-poor, laser treated fs-rGO surface to graphene-like domains. It also offers an excellent opportunity for further study of the fundamental mechanistic details of this process and exploitation of the method for industrial applications.

Preliminary studies on substrates with higher (stainless steel) and lower (air) thermal conductivities than PET are entirely consistent with the hypothesis that graphenisation is thermally mediated (not shown). Laser reduction under optimal ns-rGO conditions (0.12 J cm^{-2}, 40 pulses) on GO supported on stainless steel showed less graphenisation, while a freestanding GO film in air was completely pierced when irradiated under the same conditions. Further studies using nanosecond and femtosecond pulses are underway to better understand the effects of pulse duration and substrate thermal conductivity on graphenisation.

Preliminary studies using GAXRD support the results seen already, with laser-reduced GO showing an increased amount of the rGO phase with C (002) peak around 26° (Fig. S5 – supplementary material). Estimations of the crystallite size from this peak (using the Scherrer equation) yield a mean crystal size of 5.5–5.9 nm, indicating reasonable crystallinity. Interesting results are seen with regards to the position of the graphene oxide C (002) peak at ~11° which offers information regarding interplanar spacing, suggesting that exfoliation of graphene oxide layers may be occurring during laser reduction. Further investigation into this phenomenon is underway.

5. Conclusions

In this report, we have evaluated the photoreduction and graphenization of GO to rGO under ambient temperature and atmospheric conditions for three common laser processing approaches:

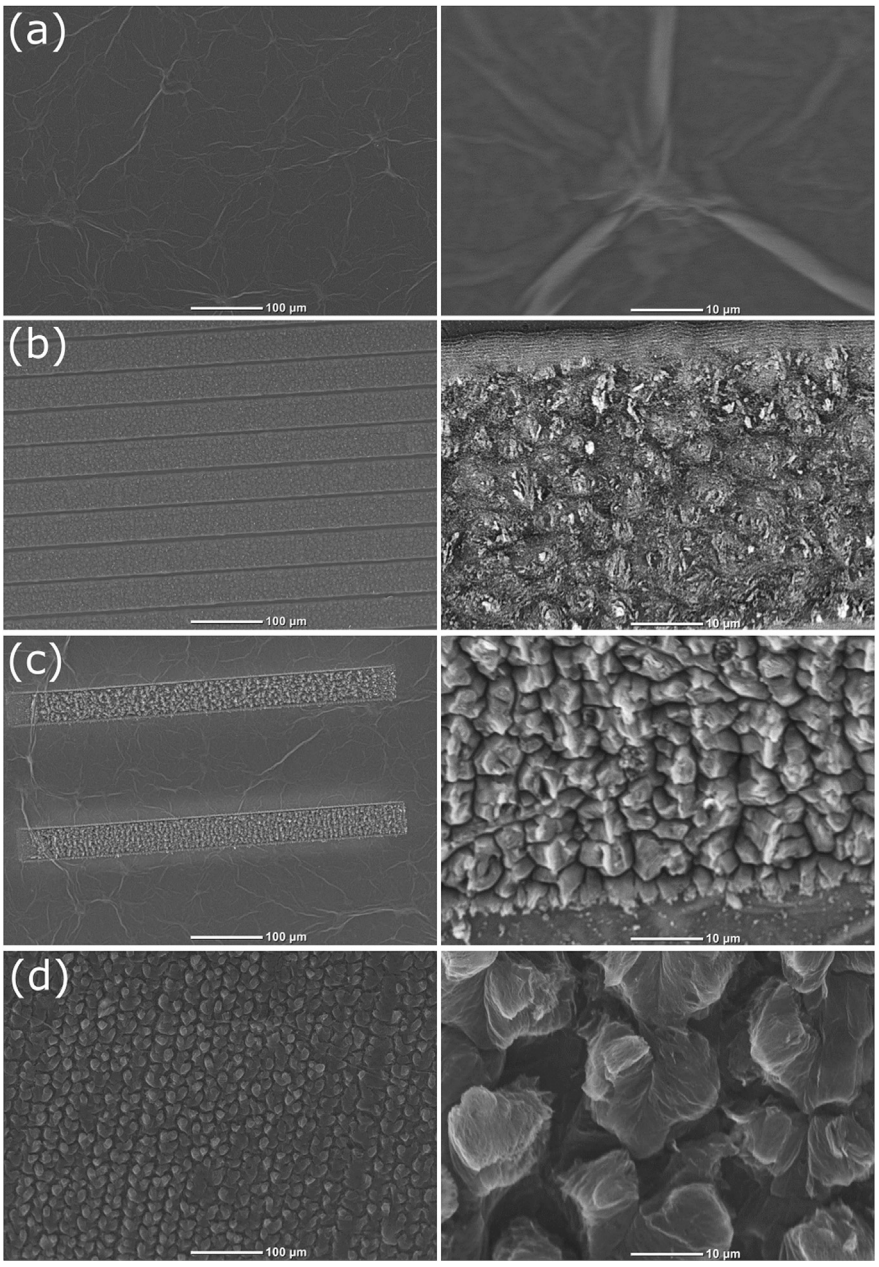

Fig. 4. SEM Images of (a) GO, (b) fs-rGO (0.15 J cm^{-2}; 40 overlapping pulses), (c) ns-rGO (0.12 J cm^{-2}; 40 overlapping pulses), and (d) cw-rGO (LightScribe maximum contrast, six passes).

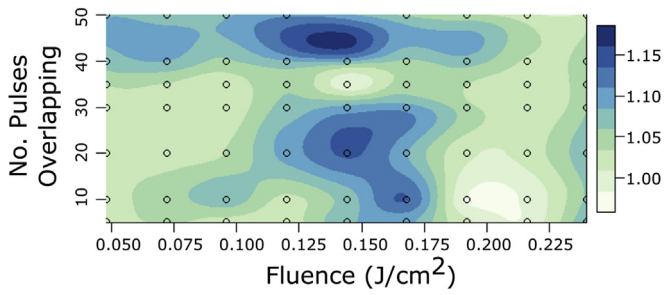

Fig. 5. The Raman I_D/I_G ratio measured on ns-rGO samples versus incident laser fluence and number of overlapping pulses. White dots represent data; contours were fit by local polynomial regression.

(1) 800 nm, 100 fs pulses, (2) 248 nm, 10 ns pulses, and (3) 788 nm CW illumination (LightScribe). To our knowledge, this is the first study of different laser processing approaches applied to the same sample under the same conditions. This approach allows a direct and robust comparison of the varied abilities of these methods to produce direct-write laser scribed graphene features in GO films, and has provided significant insight into the mechanism of the photoreduction and structural reorganization that occurs.

UV, nanosecond pulsed laser processing was the most effective at producing graphene-like rGO films, under our conditions. The optimal laser conditions for maximum oxygen removal, by XPS, and graphenization (Raman I_{2D}/I_G) with minimal defect introduction (Raman I_D/I_G) were 0.12 mJ cm^{-2} with 40 overlapping pulses. This optimal processing fluence is approximately 10-fold larger than the ablation threshold measured for GO in this study.

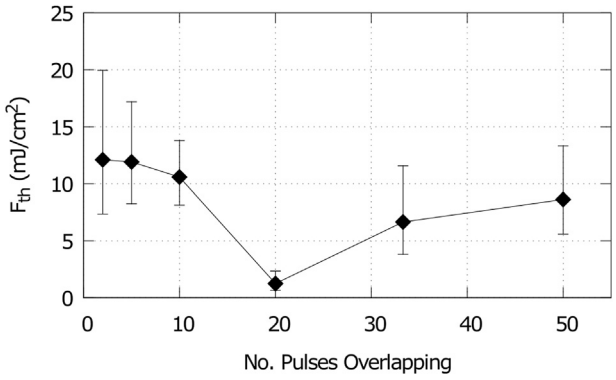

Fig. 6. The ablation threshold of GO measured using the volume regression method for 248 nm, 5 ns incident laser pulses (repetition rate 500 Hz).

800 nm, femtosecond pulsed laser processing led to removal of oxygen, but little or no graphenization (sp^3 to sp^2 reorganization) of the surface. CW illumination was found to produce relatively poor rGO materials as well; although oxygen was removed from the irradiated areas, defects were introduced concomitantly and the presence of graphene-like configurations was relatively low.

The findings reported here indicate that the laser-induced transformation of GO to rGO involves at least two steps that are mediated by distinct physical processes. The first is the laser-induced photochemical removal of oxygen from the surface. This is accompanied by laser ablation, as the transformation occurs at fluences well above the laser ablation threshold.

The second process is the structural reorganization of the newly formed, reduced carbon lattice into the planar, hexagonal, sp^2 graphene structure. The fact that we see oxygen removal but no graphenization with femtosecond irradiation indicates that this is a thermally-mediated process. Single-pulse femtosecond experiments have suggested that this structural transformation is not thermally mediated [27]. However the fact that our results were obtained for femtosecond, nanosecond and CW laser processing in parallel on the same samples under the same conditions provides strong evidence the sp^3 to sp^2 structural reorganization to a graphene-like conformation requires deposition of heat into the material, while the laser-induced, photochemical removal of oxygen from the surface does not. This is the first such comparison on a consistent GO substrate under comparable ambient conditions, and the results provide insight into the fundamental mechanism and the utility of the method for direct laser writing electronically active materials.

Acknowledgements

The authors would like to acknowledge support from the New Zealand Ministry of Business, Innovation and Employment (UOAX1202). We would also like to thank Dr. Colin Doyle (University of Auckland) for guidance in interpreting XPS results, and Professors David Geohegan (Oak Ridge National Laboratories) and Min Gu (Swinburne University of Technology) for insightful conversations at COLA 2015 in Cairns, Australia. The authors would also like to express their sincere thanks to Mr. Jay Chan and Dr. Franck Natali at Victoria University of Wellington, for their assistance with GAXRD measurements.

Appendix A. Supplementary data

Supplementary data related to this article can be found at http://dx.doi.org/10.1016/j.carbon.2015.12.038.

References

[1] K.S. Novoselov, et al., Electric field effect in atomically thin carbon films, Science 306 (5696) (2004) 666–669.
[2] M.S. Dresselhaus, P.T. Araujo, Perspectives on the 2010 nobel prize in physics for graphene, ACS Nano 4 (11) (2010) 6297–6302.
[3] M. Xu, et al., Graphene-like two-dimensional materials, Chem. Rev. 113 (5) (2013) 3766–3798.
[4] F. Bonaccorso, et al., Graphene photonics and optoelectronics, Nat. Photonics 4 (9) (2010) 611–622.
[5] M.J. Allen, V.C. Tung, R.B. Kaner, Honeycomb carbon: a review of graphene, Chem. Rev. 110 (1) (2009) 132–145.
[6] K. Novoselov, et al., Two-dimensional gas of massless Dirac fermions in graphene, Nature 438 (7065) (2005) 197–200.
[7] C. Berger, et al., Ultrathin epitaxial graphite: 2D electron gas properties and a route toward graphene-based nanoelectronics, J. Phys. Chem. B 108 (52) (2004) 19912–19916.
[8] K.R. Paton, et al., Scalable production of large quantities of defect-free few-layer graphene by shear exfoliation in liquids, Nat. Mater. 13 (6) (2014) 624–630.
[9] A. Reina, et al., Large area, few-layer graphene films on arbitrary substrates by chemical vapor deposition, Nano Lett. 9 (1) (2008) 30–35.
[10] S. Pei, H.-M. Cheng, The reduction of graphene oxide, Carbon 50 (9) (2012) 3210–3228.
[11] V.C. Tung, et al., High-throughput solution processing of large-scale graphene, Nat. Nano 4 (1) (2009) 25–29.
[12] D. Li, et al., Processable aqueous dispersions of graphene nanosheets, Nat. Nanotechnol. 3 (2) (2008) 101–105.
[13] C. Zhao, et al., Formation of uniform reduced graphene oxide films on modified PET substrates using drop-casting method, Particuology 17 (2014) 66–73.
[14] G. Eda, M. Chhowalla, Chemically derived graphene oxide: towards large-area thin-film electronics and optoelectronics, Adv. Mater. 22 (22) (2010) 2392–2415.
[15] G. Eda, G. Fanchini, M. Chhowalla, Large-area ultrathin films of reduced graphene oxide as a transparent and flexible electronic material, Nat. Nanotechnol. 3 (5) (2008) 270–274.
[16] D. Chen, H. Feng, J. Li, Graphene oxide: preparation, functionalization, and electrochemical applications, Chem. Rev. 112 (11) (2012) 6027–6053.
[17] D.R. Dreyer, et al., The chemistry of graphene oxide, Chem. Soc. Rev. 39 (1) (2010) 228–240.
[18] S. Stankovich, et al., Synthesis and exfoliation of isocyanate-treated graphene oxide nanoplatelets, Carbon 44 (15) (2006) 3342–3347.
[19] X. Zhou, et al., In situ synthesis of metal nanoparticles on single-layer graphene oxide and reduced graphene oxide surfaces, J. Phys. Chem. C 113 (25) (2009) 10842–10846.
[20] Z. Wang, et al., Direct electrochemical reduction of single-layer graphene oxide and subsequent functionalization with glucose oxidase, J. Phys. Chem. C 113 (32) (2009) 14071–14075.
[21] Y. Wang, et al., Graphene and graphene oxide: biofunctionalization and applications in biotechnology, Trends Biotechnol. 29 (5) (2011) 205–212.
[22] Y. Shao, et al., Graphene based electrochemical sensors and biosensors: a review, Electroanalysis 22 (10) (2010) 1027–1036.
[23] M. Kalbacova, et al., Graphene substrates promote adherence of human osteoblasts and mesenchymal stromal cells, Carbon 48 (15) (2010) 4323–4329.
[24] L. Wang, et al., Facile preparation of an n-type reduced graphene oxide field effect transistor at room temperature, Chem. Commun. 50 (10) (2014) 1224–1226.
[25] Z. Yin, et al., Organic photovoltaic devices using highly flexible reduced graphene oxide films as transparent electrodes, ACS Nano 4 (9) (2010) 5263–5268.
[26] M.F. El-Kady, R.B. Kaner, Scalable fabrication of high-power graphene micro-supercapacitors for flexible and on-chip energy storage, Nat. Commun. 4 (2013) 1475.
[27] X. Li, et al., Athermally photoreduced graphene oxides for three-dimensional holographic images, Nat. Commun. (2015) 6.
[28] J.T. Robinson, et al., Reduced graphene oxide molecular sensors, Nano Lett. 8 (10) (2008) 3137–3140.
[29] K.A. Mkhoyan, et al., Atomic and electronic structure of graphene-oxide, Nano Lett. 9 (3) (2009) 1058–1063.
[30] O.V. Yazyev, S.G. Louie, Electronic transport in polycrystalline graphene, Nat. Mater. 9 (10) (2010) 806–809.
[31] C. Gómez-Navarro, et al., Electronic transport properties of individual chemically reduced graphene oxide sheets, Nano Lett. 7 (11) (2007) 3499–3503.
[32] C. Gómez-Navarro, et al., Atomic structure of reduced graphene oxide, Nano Lett. 10 (4) (2010) 1144–1148.
[33] C. Ma, X. Shao, D. Cao, Nitrogen-doped graphene nanosheets as anode materials for lithium ion batteries: a first-principles study, J. Mater. Chem. 22 (18) (2012) 8911–8915.
[34] R. Mukherjee, et al., Defect-induced plating of lithium metal within porous graphene networks, Nat. Commun. (2014) 5.
[35] Q. Huang, et al., Synthesis of defect graphene and its application for room temperature humidity sensing, Mater. Lett. 83 (2012) 76–79.
[36] L. Guo, et al., Two-beam-laser interference mediated reduction, patterning

and nanostructuring of graphene oxide for the production of a flexible humidity sensing device, Carbon 50 (4) (2012) 1667–1673.
[37] Y.-H. Zhang, et al., Understanding dopant and defect effect on H 2 S sensing performances of graphene: A first-principles study, Comput. Mater. Sci. 69 (2013) 222–228.
[38] R. Trusovas, et al., Recent advances in laser utilization in the chemical modification of graphene oxide and its applications, Adv. Opt. Mater. (2015). http://onlinelibrary.wiley.com/doi/10.1002/adom.201500469/full.
[39] L. Feng, et al., A graphene functionalized electrochemical aptasensor for selective label-free detection of cancer cells, Biomaterials 32 (11) (2011) 2930–2937.
[40] H. Wang, Y.H. Hu, Graphene as a counter electrode material for dye-sensitized solar cells, Energy & Environ. Sci. 5 (8) (2012) 8182–8188.
[41] D. Luo, et al., Evaluation criteria for reduced graphene oxide, J. Phys. Chem. C 115 (23) (2011) 11327–11335.
[42] J. Liang, et al., Electromechanical actuators based on graphene and graphene/Fe3O4 hybrid paper, Adv. Funct. Mater. 21 (19) (2011) 3778–3784.
[43] X. Yu, et al., Tuning chemical enhancement of SERS by controlling the chemical reduction of graphene oxide nanosheets, ACS Nano 5 (2) (2011) 952–958.
[44] H. Huang, X. Wang, Pd nanoparticles supported on low-defect graphene sheets: for use as high-performance electrocatalysts for formic acid and methanol oxidation, J. Mater. Chem. 22 (42) (2012) 22533–22541.
[45] Y.L. Zhang, et al., Photoreduction of graphene oxides: methods, properties, and applications, Adv. Opt. Mater. 2 (1) (2014) 10–28.
[46] D.A. Sokolov, et al., Excimer laser reduction and patterning of graphite oxide, Carbon 53 (2013) 81–89.
[47] V. Strong, et al., Patterning and electronic tuning of laser scribed graphene for flexible all-carbon devices, ACS Nano 6 (2) (2012) 1395–1403.
[48] A.C. Ferrari, D.M. Basko, Raman spectroscopy as a versatile tool for studying the properties of graphene, Nat. Nanotechnol. 8 (4) (2013) 235–246.
[49] R. Trusovas, et al., Reduction of graphite oxide to graphene with laser irradiation, Carbon 52 (2013) 574–582.
[50] X. Ye, et al., Direct laser fabrication of large-area and patterned graphene at room temperature, Carbon 68 (2014) 784–790.
[51] Y. Zhang, et al., Direct imprinting of microcircuits on graphene oxides film by femtosecond laser reduction, Nano Today 5 (1) (2010) 15–20.
[52] C. Petridis, et al., Post-fabrication, in situ laser reduction of graphene oxide devices, Appl. Phys. Lett. 102 (9) (2013) 093115.
[53] D.A. Sokolov, K.R. Shepperd, T.M. Orlando, Formation of graphene features from direct laser-induced reduction of graphite oxide, J. Phys. Chem. Lett. 1 (18) (2010) 2633–2636.
[54] K. Yung, et al., Laser direct patterning of a reduced-graphene oxide transparent circuit on a graphene oxide thin film, J. Appl. Phys. 113 (24) (2013) 244903.
[55] W.S. Hummers Jr., R.E. Offeman, Preparation of graphitic oxide, J. Am. Chem. Soc. 80 (6) (1958), 1339–1339.
[56] H. Wahab, G. Xu, C. Jansing, M. Gilbert, M.F. Tesch, J. Jin, H. Timmers, Signatures of different carbon bonds in graphene oxide from soft x-ray reflectometry, X-Ray Spectrom 44 (6) (2015) 468–473.
[57] G. Speranza, L. Minati, The surface and bulk core lines in crystalline and disordered polycrystalline graphite, Surf. Sci. 600 (19) (2006) 4438–4444.
[58] J. Andrew, et al., Direct etching of polymeric materials using a XeCl laser, Appl. Phys. Lett. 43 (8) (1983) 717–719.
[59] R. Srinivasan, B. Braren, Ablative photodecomposition of polymer films by pulsed far-ultraviolet (193 nm) laser radiation: Dependence of etch depth on experimental conditions, J. Polym. Sci. Polym. Chem. Ed. 22 (10) (1984) 2601–2609.
[60] T. Deutsch, M. Geis, Self-developing UV photoresist using excimer laser exposure, J. Appl. Phys. 54 (12) (1983) 7201–7204.
[61] A. Ferrari, et al., Raman spectrum of graphene and graphene layers, Phys. Rev. Lett. 97 (18) (2006) 187401.
[62] D. Yang, et al., Chemical analysis of graphene oxide films after heat and chemical treatments by X-ray photoelectron and Micro-Raman spectroscopy, Carbon 47 (1) (2009) 145–152.
[63] L.G. Cançado, et al., Quantifying defects in graphene via Raman spectroscopy at different excitation energies, Nano Lett. 11 (8) (2011) 3190–3196.
[64] Q. Wu, et al., Femtosecond laser-induced periodic surface structure on diamond film, Appl. Phys. Lett. 82 (11) (2003) 1703–1705.
[65] W. Zhang, et al., Formation of laser-induced periodic surface structures during femtosecond laser ablation of highly oriented pyrolytic graphite (HOPG), Lasers Eng. (Old City Publ.) 25 (2013).
[66] K. Sugioka, Y. Cheng, Ultrafast lasers – reliable tools for advanced materials processing, Light Sci. Appl. 3 (2014) p. e149.
[67] X. Zhao, et al., Ultrafast carrier dynamics and saturable absorption of solution-processable few-layered graphene oxide, Appl. Phys. Lett. 98 (12) (2011) 121905.